ARTICLE IN PRESS

PERGAMON

Electrochimica Acta 00 (2002) 1–12

ELECTROCHIMICA Acta

www.elsevier.com/locate/electacta

Oxygen electrocatalysis in alkaline electrolyte: Pt(*hkl*), Au(*hkl*) and the effect of Pd-modification

T.J. Schmidt *, V. Stamenkovic, M. Arenz [1], N.M. Markovic, P.N. Ross, Jr.

Materials Sciences Division, Lawrence Berkeley National Laboratory, University of California, Berkeley, CA 94720, USA

Received 15 January 2002; received in revised form 15 April 2002

Abstract

The kinetics of the oxygen reduction reaction (ORR) was studied in alkaline electrolyte at 293–333 K on bare and Pd modified Pt(*hkl*) and Au(*hkl*) surfaces. The rotating ring-disk electrode technique was used to study the ORR with solution phase peroxide detected at the ring electrode. Pd modification was either by electrodeposition (Pt) or by vapor deposition in vacuum (Au). The surface concentration of Pd was determined in vacuum using low energy ion scattering. In agreement to the structure sensitivity found at room temperature previously, on the bare Au(*hkl*) surfaces the ORR was found to be strongly structure sensitive in the temperature range from 293 to 333 K, with order of activity being (100) ≫ (110) > (111). The structure sensitivity for Pt(*hkl*) is much less and varies in the nearly the opposite order (111) > (100) > (110). The peroxide intermediate pathway is clearly operative on Au(*hkl*) surfaces. At elevated temperature, significantly smaller amounts of peroxide are formed. The kinetics of the ORR were significantly enhanced by modification of both Pt(*hkl*) and Au(*hkl*) surfaces with Pd. The catalytic effect is most pronounced on the surfaces that are less active surfaces in the unmodified state, with enhancement at least an order of magnitude faster kinetics. Pd modification of the Au(*hkl*) surfaces, therefore, significantly reduces the structure sensitivity of the ORR. Even on the highly active Pt(111) surface the kinetics can be improved by a factor of approximately two to four due to Pd modification. The catalytic enhancement can be achieved with as little as 18 at.% Pd in the Au(*hkl*) surface. © 2002 Published by Elsevier Science Ltd.

Keywords: Oxygen reduction reaction (ORR); Surface concentration; Catalytic effect

1. Introduction

Oxygen electrochemistry is a highly interesting field in electrocatalysis due to its high importance in electrolysis and especially in electrochemical energy conversion technology (e.g. in fuel cells and batteries [1]). The strong R&D effort in fuel cell technology especially in the last decade or so has triggered numerous studies on the oxygen reduction reaction (ORR) on various materials, ranging from noble metals over transition metal oxides to organic macrocycles. For an overview we refer to several reviews: Tarasevich et al. [2] (mainly Pt, Au, and carbon), Kinoshita [1] (general overview on oxygen electrochemistry), Adzic [3] (mainly single crystal Pt and Au, organic macrocycles,) and from our laboratory [4,5] (Pt single crystals and Pt-bimetallic surfaces), respectively. However, most of the fundamental studies of the ORR have been conducted in acidic electrolyte [3–5] and primarily on Pt. ORR studies on single crystal electrodes in alkaline solution are less numerous and the individual papers must be consulted for results [6–12].

In this paper, we report temperature-dependent ORR kinetics on two types of well-defined single crystal electrodes in alkaline electrolyte: (i) pure Pt(*hkl*) and Au(*hkl*) surfaces and (ii) Pt(*hkl*) and Au(*hkl*) surfaces modified by Pd. Temperature-dependent base voltammetry is used to study surface processes on the pure noble metal electrodes. Furthermore, temperature effects on the ORR kinetics on Pt(*hkl*) and Au(*hkl*) are investigated by making use of the rotating ring–disk electrode technique which allows the quantitative separation of the two reaction products, viz., OH^- and HO_2^-. Subsequently, new kinetic results on the ORR on Pd modified Pt and Au single crystals are presented. The

* Corresponding author. Present address: Paul-Scherrer-Institut, CH-5232 Villigen-PSI, Switzerland

E-mail address: tom.schmidt@psi.ch (T.J. Schmidt).

[1] Present address: University of Bonn, Germany.

0013-4686/02/$ - see front matter © 2002 Published by Elsevier Science Ltd.

PII: S0013-4686(02)00347-X

exceptionally enhanced ORR kinetics on the Pd modified versus the unmodified surfaces presage a new era of advances in ORR electrocatalysis. The discussion section, finally, is devoted to a general comparison of the behavior of Pt-based and Au-based single crystal electrodes, i.e. in order to highlight the major similarities and differences on the pure metals with respect to oxygen electrocatalysis and the remarkable promotion of the activity of Au(*hkl*) surfaces by submonolayer amounts of Pd.

2. Experimental

2.1. Pt(hkl) and Au(hkl)

The pretreatment and assembly of the Pt(*hkl*) single crystals (0.283 cm^2) in a RRDE configuration was fully described previously [13]. In short, following flame annealing in a hydrogen flame and cooling in a stream of Ar, the single crystal was mounted into the disk position of an insertable ring disk electrode assembly (Pine Instruments). The gold single crystals (0.283 cm^{-2}) were flame annealed in a propane flame and cooled down in an Ar atmosphere before they were mounted in the RRDE setup. Subsequently, the electrodes were transferred into a thermostated standard three compartment electrochemical cell and immersed into the Ar-purged electrolyte (Ar: Bay Gas Research Purity; 0.1 M KOH: Aldrich Semiconductor Grade prepared with triply pyrodistilled water) under potentiostatic control at ≈ 0.1 V. A circulating constant temperature bath (Fischer Isotemp Circulator) maintained the temperature of the electrolyte within ± 0.5 K. All measurements were conducted nonisothermally, i.e. keeping the temperature of the reference electrode constant (≈ 298 K) while that of the working electrode was varied between 293 and 333 K. The reference electrode was a saturated calomel electrode (SCE) separated by a closed electrolyte bridge from the working electrode compartment in order to avoid chloride contamination. All potentials, however, refer to that of the reversible hydrogen electrode in the same electrolyte. The collection efficiency of the RRDE setup was $N = 0.22 \pm 5\%$. The measurements on Pt(110) were carried out on the reconstructed surface with (1×2) geometry, prepared according to ref. [14], hereafter this surfaces is denoted Pt(110) only. The reconstructed (1×2) surface was previously found to be stable in the potential range applied in the present study [14].

2.2. Pt(hkl)–Pd and Au((hkl)–Pd

Palladium films were deposited on Pt(*hkl*) via continuous potential cycling from a approximately 10^{-5} M Pd^{2+} solution in 0.05 M sulfuric acid at 50 mV s^{-}. The amount deposited was controlled by the continuous change of the voltammetric features from those characteristic of Pt(111) to those of a pseudomorphic monolayer of palladium [15,16]. After completion of a monolayer of palladium, the electrode was rinsed with water and transferred to a second electrochemical cell containing a solution (0.1 M KOH) free of Pd^{2+} ions (and emmersed at 0.1 V) where the ORR measurements were performed. Solutions were prepared from sulfuric acid (Baker Ultrex) and PdO (Alfa Products) employing pyrolytically triply distilled water.

The Au(*hkl*)–Pd electrodes were prepared and characterized in a UHV system under a base pressure of 2×10^{-10} Torr, equipped with an angular-resolving double pass cylindrical mirror analyzer (PHI-DPCMA Φ15-255GAR) with an electron source at its center axis. After several Ar^+-sputtering/annealing cycles, the cleanliness of the surfaces were checked by Auger electron spectroscopy (AES, 3 keV). AES spectra were recorded in derivative mode in the range from 140 to 600 eV using 3 keV electron beam energy, 3 eV_{p-p} modulation and -5 μA beam current. Subsequently, the crystal was cooled to liquid nitrogen temperature (77 K) and the surface was modified by vapor deposition of Pd. Different amounts of palladium were deposited onto the clean Au(*hkl*) surfaces using a UHV evaporator (Omicron/Focus, model EFM3/4), equipped with an integrated flux monitor. The deposition of Pd was followed by simultaneously recording the AES signal for Pd at 330 eV in a range of ± 10 eV. After deposition the total coverage of Pd was determined by low energy ion scattering (LEIS). LEIS spectra were taken with a He^+ beam energy of 1 keV with sample current from 5 to 30 nA at residual He pressure of 2.5×10^{-8} Torr. Scattering and incidence angle were 127 and 45°, respectively. A Φ04-303A differentially pumped ion gun was used to raster the He^+ ion beam over approximately 3×3 mm area. Time of recording was 60 s per spectrum. After Pd deposition, the crystal was allowed to thermally equilibrate with room temperature (ca. 5–6 h) and the surface composition was checked several times. Once the surface composition of the Au(*hkl*)–Pd surface alloy electrodes was found to be stable, normally after approximately 24 h, the crystals were transferred into the electrochemical cell containing 0.1 M KOH electrolyte under potential control.

3. Results

3.1. Base voltammetry of Pt(hkl) at different temperatures

In order to describe the basic principles and surface processes of the temperature dependent basic voltammetry on Pt(*hkl*) in 0.1 M KOH in the temperature

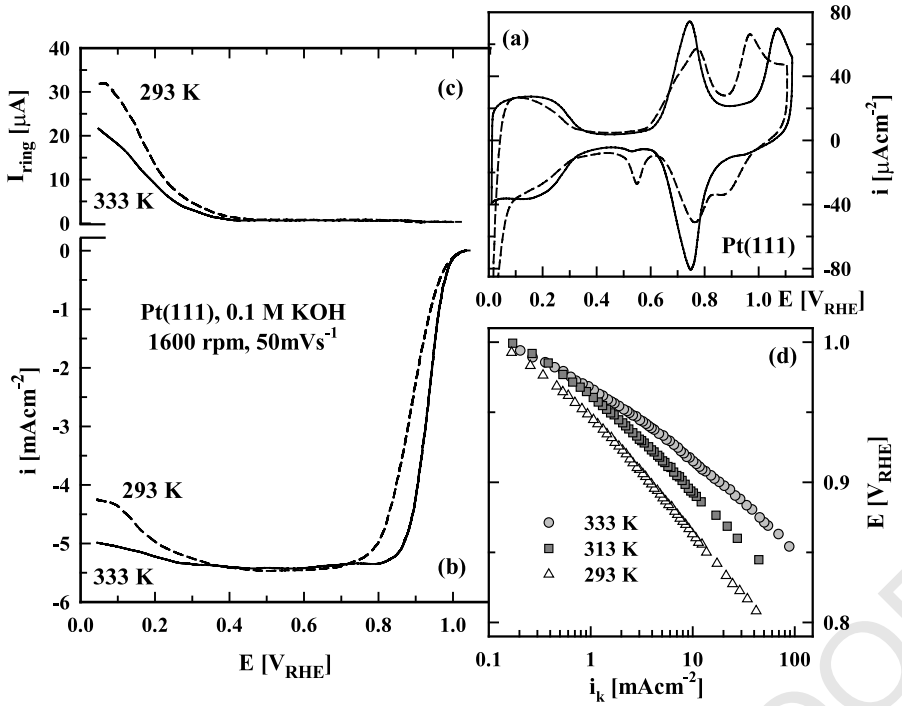

Fig. 1. (a) Base voltammetry (50 mV s^{-1}) of Pt(111) at 276 K (solid line) and 333 K (dashed line) in 0.1 M KOH. (b) ORR polarization curves (50 mV s^{-1}, 1600 rpm)) on Pt(111) at 293 K (dashed line) and 333 K (solid line). (c) Ring currents for the detection of peroxide formed during the ORR on Pt(111) at 293 K (dashed line) and 333 K (solid line). (d) Tafel plots for the ORR on Pt(111) at 293 K (white triangles), 313 K (gray squares) and 333 K (gray circles) deduced from the polarization curves at 1600 rpm.

range between 275 and 333 K, the base voltammetry of Pt(111) in 0.1 M KOH at 275 and 333 K is summarized in Fig. 1a. Since the interpretation of the temperature dependent base CV's of Pt(*hkl*) in alkaline electrolyte has been described in recent work [12,17], we only briefly review that interpretation here. Pt(111) (Fig. 1a) is the only surface of the low-index single crystals which exhibits three separate potential regions: The hydrogen underpotential deposition region (H_{upd}, $0 < E < 0.4$ V) is directly followed by the double layer region (ca. 0.4 V $< E <$ 0.6 V) and then the so-called 'butterfly region' ($0.6 < E < 0.9$ V), which is commonly assumed to represent the discharge of OH^- to form OH_{ad} [18]. In contrast to this highly reversible state of adsorbed hydroxyl, a more irreversible 'oxide' state is formed at potentials above 0.9 V. It is noteworthy, however, that the chemical state of this irreversible form of oxide is not exactly known. As already mentioned in our detailed study on temperature effects on the base CV of Pt(111) in acid and alkaline electrolyte [12], the oxide peak at approximately 1.1 V (276 K) is shifting to more negative potentials with increasing temperature. Additionally, the concomitant oxide reduction peak in the cathodic sweep direction is shifting to more positive potentials at higher temperatures, Fig. 1a. This implies that this oxidation process is becoming more reversible with increasing temperature. Although slight potential changes of the peak position of the butterfly feature are observed by increasing temperature, the formation of the reversible form of OH_{ad} is not affected significantly by temperature changes [12,17]. Similar as the reversible formation of OH_{ad} in the butterfly feature, also the H_{upd} region is only slightly affected by temperature changes. Most obviously, the adsorption of H_{upd} is shifted to more negative potentials at higher temperature. Additionally, based on the charges alone, we found a slightly lower H_{upd} coverage at 333 K than on 275 K. Details about the thermodynamics and energetics of H_{upd} and OH_{ad} on Pt(111) in alkaline solution can be found in ref. [19]. In contrast to Pt(111), which represents the only surface with 'clearly' separated potential regions for H_{upd} and OH_{ad} adsorption, a double-layer region does not exist on neither Pt(100) nor (100) and the H_{upd} region is overlapping with the OH_{ad} formation region [17]. On both surfaces the reversible formation of OH_{ad} is observed up to approximately 0.7 V, followed by a more irreversible formation of oxygenated species. Also on Pt(100) and Pt(110), the same two effects on H_{upd} and OH_{ad} is observed, i.e. the negative shift of the H_{upd} region and the increasing reversibility of the second (irreversible) oxide state. Most importantly, however, we recently demonstrated by titrating Pt(*hkl*) surfaces with the continuous oxidation of CO that some OH_{ad} must be co-adsorbed with H_{upd} even at potentials below approximately 0.1 V on all three low-index surfaces, since even at these low potentials significant CO oxidation currents could be observed. Additionally, it could be shown that the tendency to

become (irreversibly) oxidized, especially at elevated temperatures, increased in the sequence Pt(111) < Pt(100) < Pt(110) [17,20].

3.2. Oxygen reduction on Pt(hkl) in KOH

Before describing the polarization curves for the ORR in detail, a short review on the oxygen reduction reaction and the relation to RRDE measurements is given. It is well known that the ORR follows a complex reaction mechanism. Out of several propositions (for an overview we refer to ref. [1–3]), one suitable ORR reaction scheme [5], which is based on the schemes proposed by Bagotsky et al. [21] and Wroblowa et al. [22], is illustrated here.

Briefly summarized, adsorbed O_2 on the disk electrode can react either directly to OH^- (k_1-path, 4-e$^-$ reduction) or follows a serial pathway through the intermediate formation of adsorbed HO_2^- (k_2-path), which, in a second step, can be further reduced to OH^- (k_3, 2+2-e$^-$ reduction). Produced $HO_{2,ad}^-$ molecules can also desorb from the disk electrode to the solution phase (k_5-path). Additionally, $HO_{2,ad}^-$ can be chemically decomposed to form water and O_2 in a heterogeneously catalyzed reaction step (k_4-path).Without discussing this issue here, based on our previous observations [4,5] it seems that the ORR on Pt always follows the serial reaction pathway through the formation of $HO_{2,ad}^-$ (k_1 is negligible), but without producing any detectable amounts of HO_2^- in solution, i.e. $k_3 \gg k_5$. In ring–disk measurements, the solution phase intermediate HO_2^- desorbing from the electrode surface can be detected on the independently polarized Pt ring ($E_{ring} = 1.2$ V vs. RHE) electrode by oxidizing it back to O_2.

The polarization curves for the ORR on Pt(111) at 293 and 333 K (1600 rpm, 50 mV s^{-1}) are illustrated in Fig. 1b. In short, the region of mixed kinetic-diffusion control (0.8 V < E < 1 V) is followed by the diffusion limited current densities below approximately 0.8 V. At E < 0.4 V, i.e. in the H_{upd} region, a deviation of the diffusion limited currents to lower values can be observed. This deviation can be quantitatively related to the formation of HO_2^- as demonstrated by the HO_2^- detection on the ring electrode [4,11], see Fig. 1c. A more detailed discussion of the ORR in the H_{upd} region on Pt(*hkl*) can be found in our previous papers [4,11]. At lower overpotentials, i.e. in the mixed kinetic-diffusion region, no peroxide can be observed. A comparison of the ORR polarization curves at 293 and 333 K indicates that as expected considerably higher reaction rates are observed at 333 K, pointing to the fact that the ORR in KOH is a significantly activated process. The apparent activation energy, $\Delta H^{\neq}$, is 47 kJ mol^{-1} determined at constant overpotential, $\eta = 0.35$ V in an Arrhenius analysis (values summarized in Table 1) according to a procedure described previously [23,24]. A similar value was previously found in 0.05 M H_2SO_4 extrapolated to the reversible potential [25]. The logi/E-relationships (so-called Tafel plots) at 293, 313 and 333 K are plotted in Fig. 1d. The logi/E-relationships at the different temperatures were fitted by straight lines in order to determine the Tafel slopes. Decreasing Tafel slopes from approximately 86 to 57 mV per decomposition were found when going from 293 to 333 K, as summarized in Table 1. In contrast to Pt(*hkl*) in acid solution, the Tafel slopes are not proportional to RT/F. Fig. 2 illustrates the Tafel plots and the ring currents for HO_2^- formed during the ORR on Pt(100) and Pt(110), respectively. In contrast to Pt(111), some HO_2^- is detected in the potential region above 0.4 V, and there is generally a decrease of peroxide formation by increasing temperature, an increase in activity by increasing temperatures, and again decreasing Tafel slopes when going from 293 to 333 K. It is noteworthy, that on Pt(100) and Pt(110) similar apparent activation energy of approximately 42 and 37 kJ mol^{-1}, respectively, than on Pt(111) can be found. Based on the polarization curves and the Tafel plots at the different temperatures, the ORR activity increases in the order P(110)(1 × 2) < Pt(100) < Pt(111). However, in a previous study in KOH at room temperature in the same laboratory [11] a slightly different order was found, namely Pt(111) > Pt(110) > Pt(100). The discrepancy can be explained by the differences in preparation and in surface structure of the Pt(110) crystal. In the present study, we carefully prepared the reconstructed Pt(110)(1 × 2) surface, versus the unreconstructed (1 × 1) surface used in the previous study [11]. Therefore, the lower activity in the present case can be ascribed to the fact that the very 'open' Pt(110)(1 × 2) surface adsorbs OH more strongly than (1 × 1) surface in the previous study, i.e. the adsorption sites for molecular oxygen are significantly blocked by adsorbed OH (see Section 4 below).

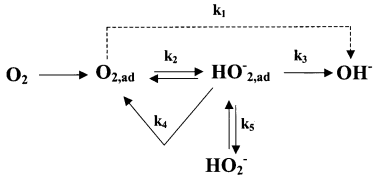

3.3. ORR on Pd modified Pt(hkl)

We had reported previously the kinetics of the ORR on Pt(111) in acid solution [15], and the effect of modification by one pseudomorphic Pd monolayer. The in situ structure of this monolayer was determined by surface X-ray scattering [16]. The ORR polarization curve in 0.1 M KOH for Pt(111)-1 ML Pd along with the polarization curve of Pt(111) is shown in Fig. 3a as an example. Quite obviously, the Pd modified Pt(111) is

Table 1
Summary of the Tafel slopes (Pt(*hkl*) and Au(*hkl*) and the apparent energies of activation (Pt(*hkl*) in 0.1 M KOH

	293 K (mV per decomposition) lcd/hcd [a]	313 K (mV per decomposition) lcd/hcd [a]	333 K (mV per decomposition) lcd/hcd [a]	$\Delta H^{\neq}$ (kJ mol^{-1}) [b]
Pt(111)	–/86	–/72	–/57	47
Pt(100)	–/112	–/78	–/60	42
Pt(110)(1 × 2)	92/190	80/120	–/83	37
Au(111)	60/185		72/150	
Au(100)	47/119		50/85	
Au(110)	44/127		37/86	

[a] Tafel slopes determined at low (lcd) and high (hcd) current densities.
[b] Determined at $\eta = 0.35$ V.

much more active for the ORR as compared with the unmodified Pt(111) surface. Additionally, at potentials below 0.4 V, smaller amounts of peroxide is formed on the Pt(111)–1 ML Pd (Fig. 3b). A comparison of Tafel plots of the modified versus the unmodified surface is illustrated in Fig. 3c. By comparing the kinetic current densities at 0.9 V, an activity improvement of a factor of approximately 4 can be observed. It is noteworthy that in perchloric acid solution Pd modified Pt is less active for the ORR [15].

3.4. Base voltammetry of Au(hkl) at different temperatures

The base voltammetry of Au(111), Au(100), and Au(110) in a temperature range between 293 and 333 K, is shown Fig. 4. This figure records the second sweep after potential excursion into the oxide region. The voltammetry at 293 K presented in Fig. 4 is characteristic for Au(*hkl*) reported previously in the literature (e.g. see ref. [7,8,26,27]). Similar to Pt(*hkl*), the base voltammetry of Au(*hkl*) is also characterized by three potential regions: (i) the 'double-layer region' at $E <$ approximately 0.6–0.7 V is followed by (ii) a region of formation of OH_{ad} up to approximately 1.1 V and (iii)

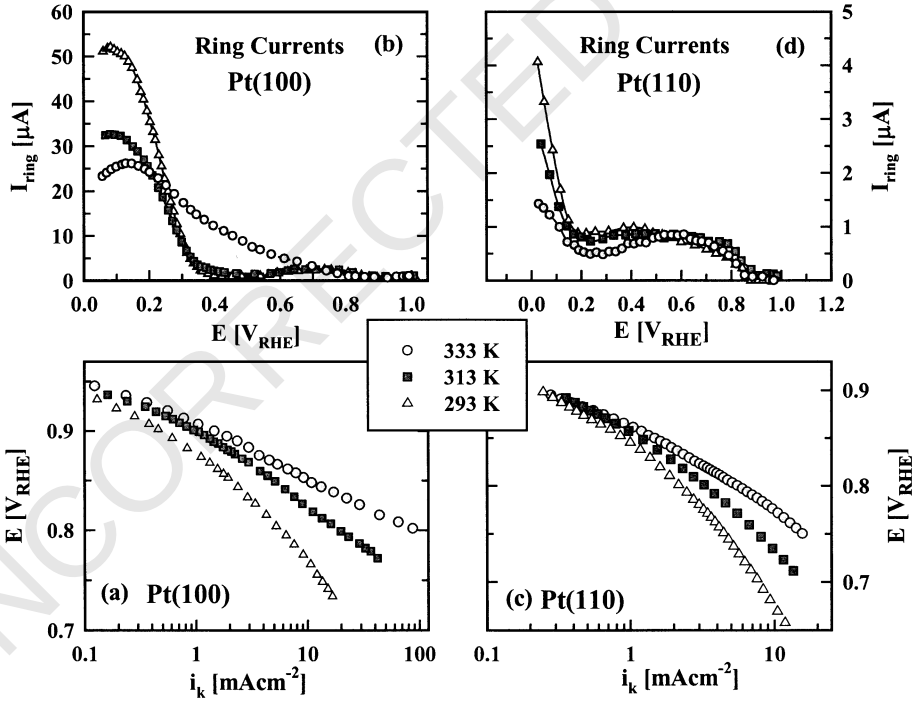

Fig. 2. (a) Tafel plots for the ORR on Pt(100) at 293 K (white triangles), 313 K (gray squares) and 333 K (gray circles) deduced from the polarization curves at 1600 rpm. (b) Ring currents for the detection of peroxide formed during the ORR on Pt(100) at 293 K (white triangles), 313 K (gray squares) and 333 K (gray circles). (c) Tafel plots for the ORR on Pt(110)(1 × 2) at 293 K (white triangles), 313 K (gray squares) and 333 K (gray circles) deduced from the polarization curves at 1600 rpm. (d) Ring currents for the detection of peroxide formed during the ORR on Pt(110)(1 × 2) at 293 K (white triangles), 313 K (gray squares) and 333 K (gray circles).

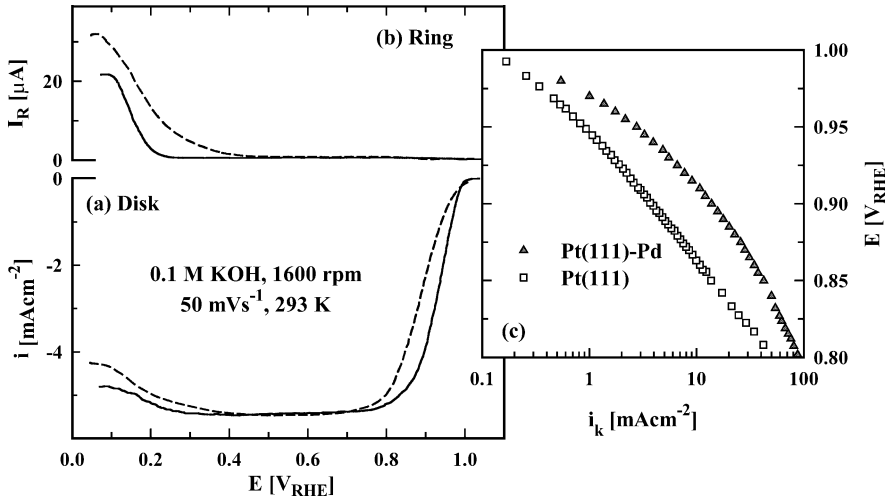

Fig. 3. (a) ORR polarization curves (50 mV s^{-1}, 1600 rpm) at 293 K on Pt(111) (dashed line) and Pt(111)-1 ML Pd (solid line) in 0.1 M KOH. (b) Ring currents for detection of peroxide species formed during the ORR ($E_{ring} = 1.2$ V). (c) Tafel plots for the ORR on Pt(111) (white squares), Pt(111)–1 ML Pd (gray triangles) in 0.1 M.

the 'oxide' formation region at $E > 1.1$ V. The reversibly adsorbed OH_{ad} is a precursor state for the formation of the surface oxide layer which starts at $E > 1.1$ V. A close comparison of the base voltammetry at 333 versus 293 K identifies systematic differences: (i) the adsorption of OH_{ad} is shifted to lower potentials by increasing temperature, i.e. the peak position for OH_{ad} adsorption is shifted by approximately 25–30 mV on Au(111) and Au(100), and approximately 80 mV on Au(110); (ii) the peak for oxide formation is shifted to more negative potentials concomitant with a shift of the oxide reduction peak in the cathodic sweep to more positive potentials by increasing temperature. That means formation/reduction of the surface oxide layer is becoming a more reversible process. It is noteworthy that the same trends can be observed on Pt(*hkl*) electrodes, see previous section and ref. [17].

Fig. 5 highlights the first sweep after emersion at approximately0.1 V of the flame annealed Au(100) crystal at 293 and 333 K, respectively. Directly after flame annealing, the Au(100) surface is hexagonally reconstructed forming a (5 × 27) unit cell [28]. Coming from the negative emersion potential, upon sweeping through the OH_{ad} region, this so-called (hex) reconstruction is lifted due to adsorption of hydroxyl species, i.e. positive of the peak at approximately 1.025 V at 293 K the Au surface has the unreconstructed (1 × 1) surface. At 333 K, due to the adsorption of OH_{ad} species at more negative potentials, the lifting of the reconstruction is also shifted to more negative potentials. The hex reconstruction reforms, albeit slowly,

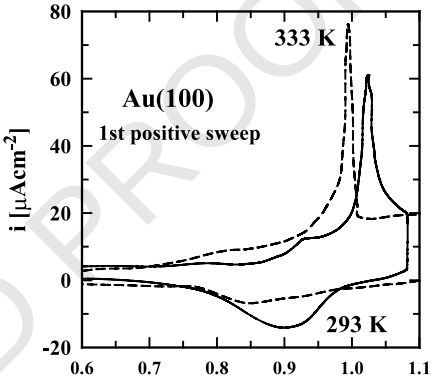

Fig. 5. Magnification of the first voltammetric sweep after emersion at ca. 0.1 V on Au(100) at 293 (solid line) and 333 K (dashed line); 0.1 M KOH, 50 mV s^{-1}.

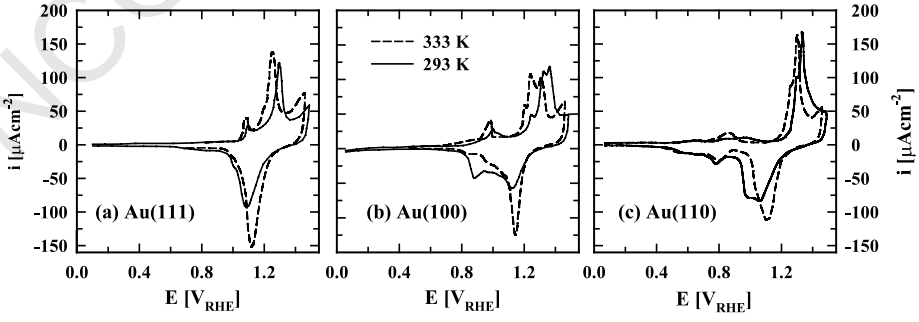

Fig. 4. Base voltammetry at 293 K (solid line) and 333 K (dashed line) on (a) Au(111), (b) Au(100) and (c) Au(110); 0.1 M KOH, 50 mV s^{-1}.

upon holding the potential < approximately 0.4 V [27]. There is a similar lifting of the reconstructed surfaces of Au(111) and (110), formed during flame annealing, when the potential is scanned above approximately 1.1 V.

3.5. Oxygen reduction on Au(hkl) in KOH

Fig. 6 summarizes the representative ORR polarization curves on Au(*hkl*) at 293 and 333 K (50 mV s^{-1}, 2500 rpm, lower panels in Fig. 6) along with the corresponding ring currents for the oxidation of peroxide formed during the ORR (upper panels). The polarization curves on Au(*hkl*) at 293 K are in agreement with previous results reported in the literature, whereas, to our knowledge, it is the first time that ORR polarization curves on Au(*hkl*) at elevated temperature are reported. The shape of the i-*E*-curves on Au(*hkl*) are qualitatively similar to those described above for Pt(*hkl*). That is, the region of mixed kinetic-diffusion control (ca. $0.7 < E < 1$ V) is followed at lower potentials by a region where the reaction is mainly under mass-transport control. However, in the region of diffusion limited current densities, no clear current plateaus for a 4-e^- process are observed as it is the case on Pt(*hkl*). Deviations from the diffusion limited current for the 4-e^- reduction to OH^- can be quantitatively related to the formation of peroxide species, as indicated by the ring currents in the upper panels. As in the case of Pt(*hkl*), less peroxide is formed by increasing the temperature to 333 K. It is clear that the ORR on Au(*hkl*) is a strongly structural sensitive process in the temperature range between 293 and 333 K, with the kinetics increasing in the order Au(111) < Au(110) ≪ Au(100). The Tafel slopes of the ORR on Au(*hkl*) at the different temperatures are summarized in Table 1. The values at room temperature are consistent with previously published Tafel slopes [6–8] with only the value for Au(111) deviating slightly. This discrepancy may be attributed to some arbitrariness in drawing the tangent through the data points that appear to be a straight line. Nevertheless, as on Pt(*hkl*), we observe decreasing Tafel slopes with increasing temperature, a fact we will focus on in the Section 4. At low current densities the Tafel slopes were found to deviate slightly form 60 mV per decomposition to lower values, which may arise from a contribution of the back reaction of the process, i.e. peroxide oxidation, which is decreasing the net current for the whole process [7].

Although well known in the literature [6,10,29], we want to emphasize the exceptional behavior of Au(100), Fig. 6c, towards the ORR. Coming from the positive potential limit, oxygen reduction occurs in essentially a 4-e^- process to form OH^-. At potentials negative of the so-called catalytic peak, a transition to an almost 2-e^- process is observed, see the polarization at 293 K in Fig. 6c. Interestingly, at 333 K the reaction takes place in a 4-e^- process in a much wider potential range and only below approximately 0.45 V are significant amounts of peroxide formed.

In order to get further insight into the reaction intermediate, i.e. solution phase HO_2^-, Fig. 7 illustrates the temperature-dependent ORR on Au(100), Fig. 7a, the corresponding ring currents for the oxidation of intermediate peroxide species, Fig. 7b, and, finally the oxidation/reduction of approximately 0.1 M KOH + 2×10^{-3} M HO_2^- (Fig. 7c). The result in Fig. 7a and c are similar to those reported previously by Adzic and co-workers [7,8]. This figure clearly demonstrates, that the ORR closely follows the reduction of HO_2^-. The activity of Au(100) for HO_2^- reduction peaks at approximately 0.2–0.8 V and above this potential only negligible amounts of peroxide are detected on the ring electrode in ORR. Below approximately 0.6 V, the

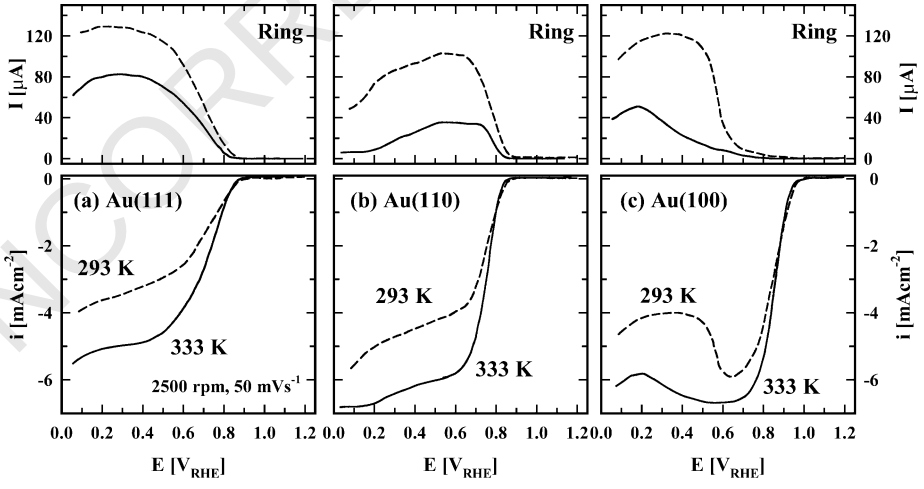

Fig. 6. ORR polarization curves (lower panel) along with the ring currents for peroxide detection (upper panel) at 293 K (dashed lines) and 333 K (solid lines) on (a) Au(111), (b) Au(110) and (c) Au(100); 0.1 M KOH, 50 mV s^{-1}, 2500 rpm.

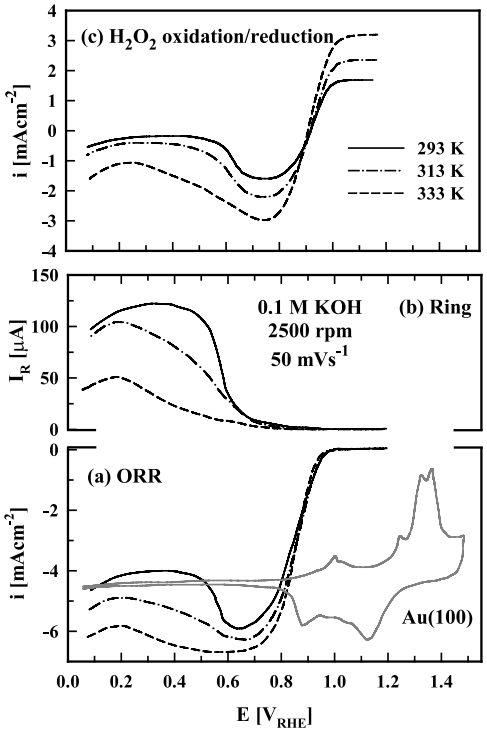

Fig. 7. (a) ORR polarization curves on Au(100), (b) ring currents for the detection of peroxide and (c) oxidation and reduction of ca. 2×10^{-3} M HO_2^- on Au(100) at 293 K (solid line), 313 K (dashed–dotted line) and 333 K (dashed line), respectively; 0.1 M KOH, 50 mV s^{-1}, 2500 rpm.

activity for HO_2^- decreases, and in the ORR there is a corresponding increase in HO_2^- production and reduction in the diffusion-limiting current. This behavior clearly points to a serial ORR mechanism through the formation of solution phase HO_2^- (2+2-e$^-$ reaction, k_2, k_3 pathway in the reaction scheme). As one can see from the polarization curves in Fig. 6, the temperature dependence in the kinetically controlled potential regions, i.e. $E > 0.8$ V, is relatively slight, much less than on Pt(*hkl*). In this narrow temperature range of 293–333 K, it was difficult to obtain an accurate measure of the activation energy and thus no activation energies are reported for Au(*hkl*). At potentials below 0.8 V, kinetics of HO_2^- reduction are significantly increased, nearly eliminating the catalytic peak at approximately 0.7 V and producing 2+2-e$^-$ reduction to much lower potentials.

3.6. ORR on Pd modified Au(hkl)

Under our experimental conditions, we never were able to form a pseudomorphic Pd monolayer on the Au(100) or Au(111) surface as reported for electrochemical Pd deposition on Au [30–33]. Even at liquid nitrogen temperature (77 K) Pd was always found to spontaneously diffuse into the Au lattice, i.e. to form a surface alloy. This effect was most pronounced on the 'open' Au(100) than on the closed packed Au(111) surface, respectively, as verified by LEIS. During thermal equilibration from approximately 77 K to room temperature, Au(*hkl*)–Pd surface alloys were formed, a phenomenon already described in ref. [34]. More complete results will be published elsewhere. Fig. 8 shows the He^+ LEIS spectrum of a Au(100)–Pd crystal after thermal equilibration at room temperature. Nominally 4 ML of Pd were evaporated at approximately 77 K. From the LEIS peak intensities, a Pd surface concentration, $x_{Pd,s}$, of approximately 0.35 (35 at.%) can be determined. The AES spectrum of the same electrode clearly shows the presence of Pd in the surface as well as the absence of carbon species, pointing to the cleanliness of the sample surface before and after the Pd deposition.

The Pd-modified Au(*hkl*) electrodes were subsequently transferred to the electrochemical cell containing 0.1 M KOH and ORR measurements were performed. Fig. 9 illustrates representative ORR polarization curves along with the ring currents for peroxide detection obtained on pure Au(100) and Au(111) (solid lines) and on Au(100)–Pd and Au(111)–Pd with different Pd surface concentrations (broken lines), respectively. By comparing the ORR polarization curves on pure Au(100) and Au(111) with the i-*E*-curves on the surfaces with $x_{Pd,s,Au(100)} \sim 0.17$ and $x_{Pd,s,Au(111)} \sim 0.18$, two striking observations can be made: (i) the onset of

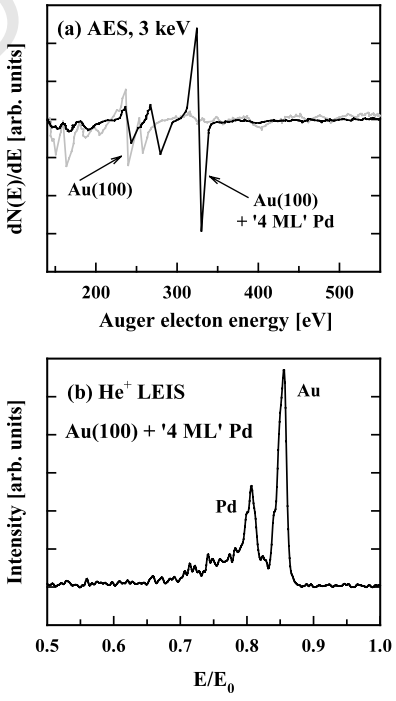

Fig. 8. (a) Auger electron spectrum (3 keV) of UHV prepared Au(100) (gray line) and Au(100) modified with Pd equivalent to 4 ML (black line). (b) LEIS spectrum of the Au(100) modified with Pd equivalent to 4 ML (He^+, $I_E = 5 \times 10^{-2}$ mA, 1 keV), resulting in ca. 35% Pd in the surface.

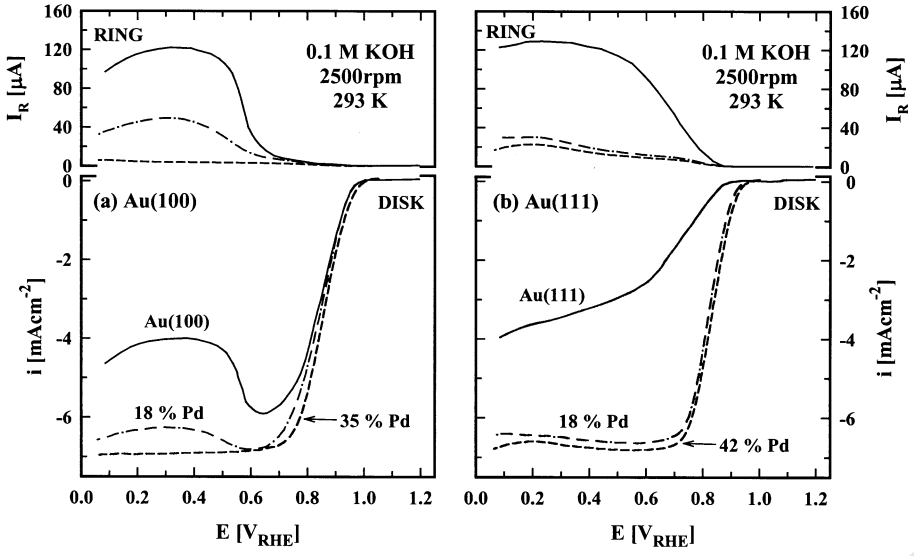

Fig. 9. (a) ORR polarization curves on pure Au(100) (solid line), Au(100)–17% Pd (dashed–dotted line, 1 ML Pd) and Au(100)–35% Pd (dashed line, 4 ML Pd) along with the ring currents for the detection of peroxide (upper panel). (b) ORR polarization curves on pure Au(111) (solid line), Au(111)–18% Pd (dashed–dotted line, 1 ML Pd) and Au(111)–42% Pd (dashed line, 2 ML Pd) along with the ring currents for the detection of peroxide (upper panel); 0.1 M KOH, 50 mV s^{-1}, 2500 rpm, 293 K.

oxygen reduction is shifted to more positive potentials, i.e. the Pd-modified surface is more active than the unmodified surface, and (ii) the formation of HO_2^- is significantly reduced on the Pd-containing Au(*hkl*) surfaces. Both effects are most pronounced on Au(111)–18% Pd, where not only a catalytic shift at the ORR onset of approximately 120 mV versus pure Au(111) is observed, but also a transition of the reaction from an almost pure 2-e^- process (HO_2^- formation) to an almost 4-e^- process (OH^- formation) on the Pd-modified surface is observed. Increasing the Pd surface concentrations to $x_{Pd,s,Au(100)} \sim 0.35$ and $x_{Pd,s,Au(111)} \sim 0.42$ still improves the electrocatalytic properties of the Au(*hkl*)–Pd surfaces with an increase in activity combined with a shift to almost 100% selectivity towards the formation of OH^-.

4. Discussion

4.1. ORR on Pt(*hkl*) and Au(*hkl*)

We will discuss the results on Pt(*hkl*) and Au(*hkl*) in terms of the elementary steps derived from the generalized reaction scheme for oxygen reduction in alkaline solution given in the previous section:

$$O_2 \rightarrow (O_2)_{ad} \quad (1)$$

$$(O_2)_{ad} + 1e^- \rightarrow (O_2^-)_{ad} \quad (1a)$$

$$(O_2)_{ad} + H_2O \rightarrow (HO_2^-)_{ad} + OH_{ad} \quad (1b)$$

$$(HO_2^-)_{ad} = HO_2^- \quad (2)$$

$$(HO_2^-)_{ad} = O_{ad} + OH_{ad} \quad (3a)$$

$$O_{ad} + H_2O + 1e^- \rightarrow OH_{ad} + 2OH^- \quad (3b)$$

$$OH_{ad} + 1e^- = OH^- (x2) \quad (4)$$

For Pt surfaces, steps Eqs. (1a) and (1b) are generally considered to be rate determining, and are often written as a single reaction in which $(O_2^-)_{ad}$ does not appear explicitly. But such a reaction is not an elementary step, and writing such a reaction simply means that the elementary steps Eqs. (1a) and (1b) proceed at the same rate. Likewise Eqs. (3a) and (3b) are often combined to yield a single 1 e^- step in which O_{ad} does not appear explicitly, but again this would not be an elementary step. With Eqs. (1a) and (1b) rate determining, steps (2)–(4) are at equilibrium. Careful comparisons of voltammetry on Pt surfaces with and without O_2 in solution have shown that at all potentials the coverage by OH_{ad} is unchanged by the presence of O_2, i.e. it is determined entirely by the equilibrium constant of step (4). This implies that the equilibria for steps (Eqs. (3a), (3b) and (4)) are shifted strongly to the right hand side, and that the coverage by $(HO_2^-)_{ad}$ in particular is low, as is the amount of HO_2^- in solution. The mechanism is very useful in establishing the role of OH_{ad} in the structure sensitivity of the reaction on Pt(*hkl*). Stronger adsorption of OH_{ad} causes the rate of Eqs. (1a) and (1b) to 'back up' due to the accumulation of OH_{ad} on the surface, blocking sites for electron transfer to O_2. The structure sensitivity then follows the relative strengths of adsorption of OH_{ad} and the OH_{ad} adsorption isotherm, (110) > (100) > (111) [17,20], with the reaction rates then varying in reverse proportion, (111) > (110) > (100). However, examination of the kinetic parameters for the ORR in Table 1 reveals that this analysis might be an oversimplification, and does not necessarily capture all of the factors that contribute to the structure

sensitivity. Although the apparent activation energies for all low-index Pt(*hkl*) surfaces are very similar in the range between 37 and 47 kJ mol^{-1}, the Tafel slopes are different on all three surfaces. In line with the OH_{ad} site blocking effect discussed above, it should be noted that above a certain OH_{ad} coverage not enough adsorption sites are present on the surface, and, hence, a change in the rate determining step from reaction (Eq. (1a)), the first electron transfer, to the O_2 adsorption process, reaction (1), can be expected. That this is indeed the case shows the least active Pt(110) electrode, were the ORR proceeds on a surface highly covered by oxygenated species concomitant with the very high Tafel slopes above 130 mV per decomposition observed on this surface, see Table 1, which directly points to a chemical rate determining step, e.g. reaction (1). However, a full explanation of the structure sensitivity of the ORR on Pt(*hkl*) in alkaline electrolyte will await a more quantitative kinetic model than we can offer at this time.

On other surfaces, such as the Au(111) and (110) surfaces studied here, HO_2^- appears in solution at the same potential where O_2 is reduced, and there is no measurable amount of O_2 reduced without the production of HO_2^- in solution (Fig. 6). However, the reduction is not exclusively to peroxide, as the ring-disk measurement indicates $n > 2$, typically 3 ± 0.5. Relative to the Pt surfaces, if we assume the same mechanism and rate determining step, the difference in activity could qualitatively be attributed to the much weaker interaction of OH_{ad} and O_{ad} on the Au surface, causing an accumulation of HO_2^- both on the surface and in solution. The base voltammetry shown in Fig. 4 clearly shows that indeed there is a much weaker adsorption energy for OH_{ad} and O_{ad} on the Au(*hkl*) surfaces than for the Pt(*hkl*) surfaces, with the onset of OH formation shifted by more than +0.4 V for each crystal face. Au(100) is the exception in terms of ORR activity, having 'Pt-like' activity in the potential region above 0.8 V, without the production of any peroxide in solution, i.e. 4-e^- reduction. Taylor et al. [10] pointed out that the Pt-like behavior is dependent on the electrode pre-history, and is observed only on the negative going sweep from potentials above approximately 1.1 V. They postulated two possible explanations: (a) the (100) surface is un-reconstructed above 1.1 V and becomes reconstructed upon reducing the potential below approximately 0.6 V, this transition causing the catalytic peak in the polarization curve around 0.7 V; (b) surface oxide produced at potentials above 1.1 V are actually catalytic for the ORR and their reduction from the surface below approximately 0.6 V causes the catalytic peak. In a later study from this laboratory [27], we found from in situ surface X-ray scattering (SXS) that there is no structural transition on the Au(100) surface on the negative going sweep from 1.1 V in the potential region around 0.6–0.8 V, i.e. the surface remains in the un-reconstructed (1×1) geometry. A catalytic effect of the (relatively) irreversible oxide formed above 1.1 V is against chemical intuition, and furthermore at 333 K there is essentially no 'oxide' left on the surface at 0.8–0.9 V (Fig. 4b) but the region of 4-e^- reduction is extended to even lower potentials. So an explanation for the unique behavior of the Au(100) for the ORR in alkaline solution remains elusive.

Finally, at the end of this section we want to discuss briefly the Tafel slopes on Pt(*hkl*) and Au(*hkl*) as summarized in Table 1. Most notably, independent of the exact value of the Tafel slopes, one trend can clearly be observed: on both Pt(*hkl*) and Au(*hkl*) the Tafel slopes are always decreasing with increasing temperature. This result is in the contrast to Pt(*hkl*) in acid electrolyte, where the Tafel slopes increase with the temperature, viz., from 116 mV per decomposition at 293 K to 132 mV per decomposition at 333 K as expected [4,5]. One explanation for decreasing Tafel slopes with increasing temperature is a temperature dependence of the apparent transfer coefficient, α, as discussed and summarized by Adzic [3]. It is also possible to derive anomalous temperature dependence in the Tafel slope even when α is not temperature dependent. Assuming step Eq. (1a) as the rate-determining step one may write the rate expression according to [2,19,35]

$$i = nFKc_{O2}(1 - \Theta_{OH})\exp\left(\frac{-\alpha FE}{RT}\right)\exp\left(\frac{-\gamma r_{OH}\Theta_{OH}}{RT}\right) \quad (5)$$

with Θ_{OH} being the potential dependent coverage of OH_{ad}, α and γ the temperature independent transfer coefficients ($= 0.5$ in this case), n the number of exchanged electrons ($n = 1$ in this case), F the Faraday constant, c_{O2} the oxygen concentration, K a constant including all chemical parameters, and r_{OH}/RT the so called Frumkin parameter describing either repulsive or attractive interactions between adsorbates. The first exponential term denotes exactly a Butler–Volmer term. If one includes only the coverage dependence of the pre-exponential term (i.e. $r_{OH} = 0$), OH adsorption is assumed to follow a Langmuir isotherm; if $r_{OH} \neq 0$, the adsorption proceeds according to a Frumkin isotherm with lateral interactions of the adsorbates. The Tafel slopes at constant temperature, say 293 K, expected from this model should deviate from the 116 mV per decomposition towards smaller values depending of r_{OH} (under both Langmuirian and Frumkin conditions). That means, in order to model decreasing Tafel slopes with increasing temperatures, the $(1-\Theta_{OH})$ term and/or the Frumkin-term must overcompensate the Butler–Volmer term. Consequently, in order to fit the experimental Tafel slopes using the experimental OH_{ad} adsorption isotherms (in the absence of O_2 [17]),

mathematically one has to include r_{OH} values that increase with the temperature. We recall that higher r_{OH} values describe stronger repulsive interactions of the adsorbates (= lower free energy of adsorption at given coverage), and increasingly stronger interactions with increasing temperature is consistent with chemical intuition. Nonetheless, the effect of decreasing Tafel slopes with increasing temperature still need further theoretical modeling in order to reach unambiguous conclusions.

4.2. ORR on Pt(hkl)–Pd and Au(hkl)–Pd

The modification of Pt(111) with one ML of Pd and the formation of Au(*hkl*)–Pd surface alloys leads to significant enhancements of the ORR kinetics. On Pt(111), the enhancement is relatively small, e.g. factors of 2–4, but on Au(111) the enhancement is more than an order of magnitude. On Au(111), the half-wave potential is shifted approximately 90 mV more positive with respect to unmodified Au(111) with only 18% at.% Pd on the surface. Additionally, the reaction on the modified Au(111) surface proceeds nearly entirely in a 4-e^- process, whereas on pure Au(111) the reaction proceeds exclusively via solution phase peroxide. The enhancement by Pd appears to saturate at less than 1 ML coverage, implying that there is a synergistic effect of Pd, i.e. the activity per surface Pd atom goes through a maximum at a surface concentration between 20 and 50 at.%. It appears from cyclic voltammetric measurements that Pt(111)–1 ML Pd is a slightly more 'oxophilic' surface than pure Pt(111). Also the base CV's of Au(*hkl*)–Pd show that these surfaces are more 'oxophilic' than pure Au(*hkl*) surfaces. That is, for both Pt–Pd [36] and Au–Pd [37], respectively, the adsorption of OH_{ad} starts at much more negative potentials than observed on the unmodified surfaces, identical to the behavior of the Pt–Pd system in perchloric acid solution [38]. Recent theoretical calculations by Liu and Norskov [39] also showed that the interaction of oxygen with Pd–Au surface alloys is increasing with increasing Pd surface concentration. In line with the previous observation of the catalytic activity of OH_{ad} for the ORR on Au(100) [7], it appears that on the Pd-modified relative to the unmodified surfaces the electronic surface properties are changed in a way that a catalytic OH_{ad} state can be formed in conjunction with the Pd adatom. We want to emphasize, however, that we are still in progress of collecting and evaluating our data on the Pd-modified surfaces, and more work is needed for a better understanding of these significant catalytic effects. The catalytic improvements found on the Pd-modified Pt(*hkl*) and Au(*hkl*) surfaces, however, are important new observations which may help in the pursuit of new ORR catalysts.

5. Conclusion

The kinetics of oxygen reduction in alkaline electrolyte was studied on bare and Pd modified Pt(*hkl*) and Au(*hkl*) surfaces using the rotating ring–disk electrode technique with solution phase peroxide detected at the ring electrode. Pd modification was either by electrodeposition (Pt) or by vapor deposition in vacuum (Au). The surface concentration of Pd was determined in vacuum using low energy ion scattering. On the bare Au(*hkl*) surfaces the ORR was found to be strongly structure sensitive in the temperature range from 293 to 333 K, with order of activity being (100) ≫ (110) > (111). The structure sensitivity for Pt(*hkl*) is much less and varies in the nearly the opposite order (111) > (100) > (110) over the same temperature range. The peroxide intermediate pathway is clearly operative on Au(*hkl*) surfaces. At elevated temperature, significantly smaller amounts of peroxide are formed on both Au(*hkl*) and Pt(*hkl*), respectively.

The kinetics of the ORR were significantly enhanced by modification of both Pt(*hkl*) and Au(*hkl*) surfaces with Pd. The catalytic effect is most pronounced on the surfaces that are less active surfaces in the unmodified state, with enhancement at least an order of magnitude faster kinetics. Pd modification of the Au(*hkl*) surfaces, therefore, significantly reduces the structure sensitivity of the ORR. Even on the highly active Pt(111) surface the kinetics can be improved by a factor of approximately 2–4 due to Pd modification. The catalytic enhancement can be achieved with as little as 18 at.% Pd in the Au(*hkl*) surface.

Acknowledgements

This work was supported by the Assistant Secretary for Conservation and Renewable Energy, Office of Transportation Technologies, Electric and Hybrid Propulsion Division of the US Department of Energy under Contract No. DE-AC03-76SF00098. One of us (M.A) is grateful to the Deutscher Akademischer Austauschdienst (DAAD) for a travel grant.

References

[1] K. Kinoshita, Electrochemical Oxygen Technology, Wiley, New York, 1992.
[2] M.R. Tarasevich, A. Sadkowski, E. Yeager, in: J.O. Bockris, B.E. Conway, E. Yeager, S.U.M. Khan, R.E. White (Eds.), Comprehensive Treatise in Electrochemistry, Plenum Press, New York, 1983, p. 301.
[3] R.R. Adzic, in: J. Lipkowski, P.N. Ross (Eds.), Electrocatalysis, Wiley-VCH, New York, 1998, p. 197.

[4] N.M. Markovic, P.N. Ross, Jr., in: A. Wieckowski (Ed.), Interfacial Electrochemistry-Theory, Experiments and Applications, Marcel Dekker, New York, 1999, p. 821.
[5] N.M. Markovic, T.J. Schmidt, V. Stamenkovic, P.N. Ross, Fuel Cells 1 (2001) 105.
[6] R.R. Adzic, N.M. Markovic, J. Electroanal. Chem. 138 (1982) 443.
[7] R.R. Adzic, N.M. Markovic, V.B. Vesovic, J. Electroanal. Chem. 165 (1984) 105.
[8] N.M. Markovic, R.R. Adzic, V.B. Vesovic, J. Electroanal. Chem. 165 (1984) 121.
[9] N.A. Anastasijevic, Z.M. Dimitijevic, R.R. Adzic, Electrochim. Acta 31 (1986) 1125.
[10] E.J. Taylor, N.R.K. Vilambi, A. Gelb, J. Electrochem. Soc. 136 (1989) 1939.
[11] N.M. Markovic, H.A. Gasteiger, P.N. Ross, J. Phys. Chem. 100 (1996) 6715.
[12] N.M. Markovic, T.J. Schmidt, B.N. Grgur, H.A. Gasteiger, P.N. Ross, Jr., R.J. Behm, J. Phys. Chem. B 103 (1999) 8568.
[13] N.M. Markovic, H.A. Gasteiger, P.N. Ross, J. Phys. Chem. 99 (1995) 3411.
[14] N.M. Markovic, B.N. Grgur, C.A. Lucas, P.N. Ross, Surf. Sci. 384 (1997) L805.
[15] V. Climent, N.M. Markovic, P.N. Ross, J. Phys. Chem. B 104 (2000) 3116.
[16] N.M. Markovic, C.A. Lucas, V. Climent, V. Stamenkovic, P.N. Ross, Surf. Sci. 465 (2000) 103.
[17] T.J. Schmidt, N.M. Markovic, P.N. Ross, Jr., J. Phys. Chem. B 105 (2001) 12082.
[18] F.T. Wagner, P.N. Ross, Jr., J. Electroanal. Chem. 250 (1988) 301.
[19] N.M. Markovic, H.A. Gasteiger, B.N. Grgur, P.N. Ross, J. Electroanal. Chem. 467 (1999) 157.
[20] T.J. Schmidt, N.M. Markovic, P.N. Ross Jr., J. Electroanal. Chem. (2001), in press
[21] V.S. Bagotzky, M.R. Tarasevich, V.Y. Filinovskij, Lektrokhimiya 5 (1969) 1218.
[22] H.S. Wroblowa, Y. Pan, G. Razumney, J. Electroanal. Chem. 69 (1976) 195.
[23] A. Parthasarathy, S. Srinivasan, A.J. Appleby, C.R. Martin, J. Electrochem. Soc. 139 (1992) 2530.
[24] U.A. Paulus, T.J. Schmidt, H.A. Gasteiger, R.J. Behm, J. Electroanal. Chem. 495 (2001) 134.
[25] B.N. Grgur, N.M. Markovic, P.N. Ross, Jr., Can. J. Chem. 75 (1997) 1465.
[26] A. Hamelin, M.J. Sottomayor, F. Silva, S.C. Chang, M.J. Weaver, J. Electroanal. Chem. 295 (1990) 291.
[27] I.M. Tidswell, N.M. Markovic, C.A. Lucas, P.N. Ross, Jr., Phys. Rev. B 47 (1993) 16542.
[28] D.M. Kolb, Prog. Surf. Sci. 51 (1996) 109.
[29] N.M. Markovic, I.M. Tidswell, P.N. Ross, Langmuir 10 (1994) 1.
[30] M. Baldauf, D.M. Kolb, Electrochim. Acta 38 (1993) 2145.
[31] H. Naohara, S. Ye, K. Uosaki, J. Phys. Chem. B 102 (1998) 4366.
[32] H. Naohara, S. Ye, K. Uosaki, J. Electroanal. Chem. 473 (1999) 2.
[33] L.A. Kibler, M. Kleinert, R. Randler, D.M. Kolb, Surf. Sci. 443 (1999) 19.
[34] B.E. Koel, A. Sellidj, M.T. Paffett, Phys. Rev. B 46 (1992) 7846.
[35] F.A. Uribe, G. Wilson, T. Springer, S. Gottesfeld, in: D. Scherson, D. Tryk, M. Daroux, X. Xing (Eds.), Structural Effects in Electrocatalysis and Oxygen Electrochemistry, PV 92-11, The Electrochemical Society, Pennington, NJ, 1991, p. 494.
[36] M. Arenz, V. Stamenkovic, T.J. Schmidt, K. Wandelt, P.N. Ross, N.M. Markovic, Surf. Sci., in press.
[37] M. Arenz, V. Stamenkovic, T.J. Schmidt, N.M. Markovic, P.N. Ross Jr., in preparation.
[38] T.J. Schmidt, N.M. Markovic, V. Stamenkovic, P.N. Ross Jr., G.A. Attard, D.J. Watson, submitted for publication.
[39] P. Liu, J.K. Norskov, Phys. Chem. Chem. Phys. 3 (2001) 3814.